Energy 59 (2013) 689–697

Contents lists available at ScienceDirect

Energy

journal homepage: www.elsevier.com/locate/energy

Geometry optimization of thermoelectric coolers using simplified conjugate-gradient method

Yu-Xian Huang [a,b], Xiao-Dong Wang [a,c,*], Chin-Hsiang Cheng [d], David Ta-Wei Lin [e]

[a] State Key Laboratory of Alternate Electrical Power System with Renewable Energy Sources, North China Electric Power University, Beijing 102206, China
[b] Department of Mechanical Engineering, National Chung Cheng University, Chiayi 62102, Taiwan
[c] Beijing Key Laboratory of Multiphase Flow and Heat Transfer for Low Grade Energy, North China Electric Power University, Beijing 102206, China
[d] Department of Aeronautics and Astronautics, National Cheng-Kung University, Tainan 70101, Taiwan
[e] Institute of Mechatronic System Engineering, National University of Tainan, Tainan 700, Taiwan

ARTICLE INFO

Article history:
Received 25 March 2013
Received in revised form
25 June 2013
Accepted 27 June 2013
Available online 27 July 2013

Keywords:
Thermoelectric cooling
Numerical modeling
Coupling of temperature and electric potential
Simplified conjugate-gradient method
Optimization

ABSTRACT

This paper develops an inverse problem approach to optimize the geometric structure of TECs (thermoelectric coolers). The approach integrates a complete multi-physics TEC model and a simplified conjugate-gradient method. The present TEC model couples the heat and electrical conductions and accounts for all physical mechanisms occurred within TECs. Three geometric parameters, the semiconductor pair number, N, leg length of semiconductor column, H_{pn}, and base area ratio of semiconductor columns to TEC, γ, are optimized simultaneously at fixed current and fixed temperature difference. The cooling rate on the cold end is the objective function to be maximized to obtain the optimal TEC geometry. The effects of applied current and temperature difference on the optimal geometry are discussed. The results show that at temperature difference of 20 K, the geometry optimization increases the TEC cooling rate by 1.99–10.21 times compared with the initial TEC geometry, and the optimal N decreases from 100 to 47 with invariable $\gamma = 0.95$ and $H_{pn} = 0.2$ mm, as the applied current varies from 1.0 A to 3.0 A. With the increase in temperature difference, the optimal N increases at smaller currents of $I \leq 1.0$ A, however, it is almost invariable at larger currents of $I \geq 1.5$ A.

1. Introduction

Thermoelectric devices can be classified into two different groups: one is the TEG (thermoelectric generator) which converts heat into electricity by Seebeck effect [1–3] and the other is the TEC (thermoelectric cooler) which converts electricity into heat by Peltier effect [4,5]. In the recent years, as the thermoelectric materials have been progressed remarkably, the TEC attracts more and more attention because it do not use any moving parts and environmentally harmful fluids as well as it has high reliability and simplicity [6,7].

A TEC is composed of a number of semiconductor element pairs which are connected electrically in series and thermally in parallel, and each pair includes a p-type semiconductor column and an n-type semiconductor column. The cooling performance of the TEC strongly depends on thermoelectric materials. The most important performance index of thermoelectric materials is the figure of merit (ZT) which is defined by $ZT = \alpha^2 T\sigma/k$, where α is the Seebeck coefficient, T is the absolute temperature, σ is the electrical conductivity, and k is the thermal conductivity of the material. A higher ZT value will lead to a better TEC performance, thus, high α and σ, as well as low k are desired for thermoelectric materials [6,7].

The investigations also found that the geometric structure has remarkable effects on the TEC and TEG (thermoelectric generator) performance [8–23]. Chen et al. [21] proposed a new cycle model consisting of a multi-couple thermoelectric device and involving several key irreversibilities of real TEGs. They used the model to optimize the performance of a multi-couple TEG and discussed the optimal structure of the TEG. Chen [22] investigated the theoretical maximum efficiency of solar TEG by using Lagrangian multiplier method. For a specific TEC with a fixed base area, the geometric parameters include the semiconductor pair number, the leg length (or height of semiconductor column), and the base area ratio of semiconductor columns to TEC. All parameters have coupled effect on the TEC performance. Although an individual parameter study is useful but it cannot answer how one can obtain

* Corresponding author. Beijing Key Laboratory of Multiphase Flow and Heat Transfer for Low Grade Energy, North China Electric Power University, Beijing 102206, China. Tel./fax: +86 10 62321277.
E-mail address: wangxd99@gmail.com (X.-D. Wang).

0360-5442/$ – see front matter © 2013 Elsevier Ltd. All rights reserved.
http://dx.doi.org/10.1016/j.energy.2013.06.069

the optimal TEC structure. Thus, a multi-parameter coupled/combined effect should be considered to reach the optimal TEC performance.

Cheng et al. combined a TEC model and a genetic algorithm to optimize the geometry and performance of the single-stage [23] and two-stage TEC [12]. In their study, the leg length, the leg area and the number of legs were taken as the search variables and were optimized simultaneously to reach the maximum cooling rate under the requirement of minimum COP (coefficient of performance) and the restriction on the maximum cost of the material. In their studies, the standard energy equilibrium model (the zero-dimensional model) was used as the direct problem solver, where only the heat balance equations at the hot and cold ends were solved. The advantage of the zero-dimensional model is that it can obtain the analytical expressions for the TEC performance, but its accuracy is limited due to grossly simplifying assumptions. For example, Joule heat and Thomson heat are assumed to be equally distributed to the hot and cold ends, and only the constant or temperature-averaged material properties can be used. It is well known that the direct problem solver is very critical for an optimization approach. If the direct problem solver is not enough accurate, the optimal geometry cannot be obtained by such optimization approach.

Recently, we developed a general, three-dimensional numerical model of thermoelectric devices [24], in which the heat conduction equation and the electric potential equation were solved coupled and all thermoelectric effects were taken into account, including Seebeck effect, Peltier effect, Thomson effect, Joule heating, Fourier's heat conduction, and heat loss to the ambient. The model is different from the previous models [8–20], in these models only the one- or three-dimensional heat conduction equation with Joule heat and/or Thomson heat as internal heat sources was solved, but electric potential equation was ignored based on the assumption of uniform current density across the semiconductor cross-section.

The objective of this work is to develop an inverse problem approach to look for the optimal TEC geometry, which integrates our previous TEC model [24] and a simplified conjugated-gradient method. The simplified conjugated-gradient method was originally proposed by Cheng et al. [25] and has been applied successfully to optimize the geometric structures of proton exchange membrane fuel cells [26–28], micro-channel heat sinks [29,30], and shell-and-tube heat exchangers [31] in our previous studies. The semiconductor pair number, the leg length, and the base area ratio of semiconductor columns to TEC as search variables are optimized to reach the maximum TEC cooling rate at a fixed applied current and a fixed temperature difference between the cold and hot ends. Then the effects of the applied current and the temperature difference on the optimal TEC geometry are discussed. The present optimization approach and the corresponding results are expected to provide a guide to the practical TEC design.

2. Optimization approach

2.1. Optimized geometric parameters

Fig. 1a shows the schematic of a TEC, which has a base area of A_{total} and is composed of N semiconductor pairs. A single pair includes a p-type semiconductor column and an n-type semiconductor column, three metallic interconnectors, and two electrically insulating ceramic plates. The p-type and n-type semiconductor columns have the same leg length of H_{pn}. It is noted that the Seebeck coefficients, electrical conductivities and thermal conductivities of p-type and n-type materials in the TEC are different from each other. Thus, a better TEC design should have

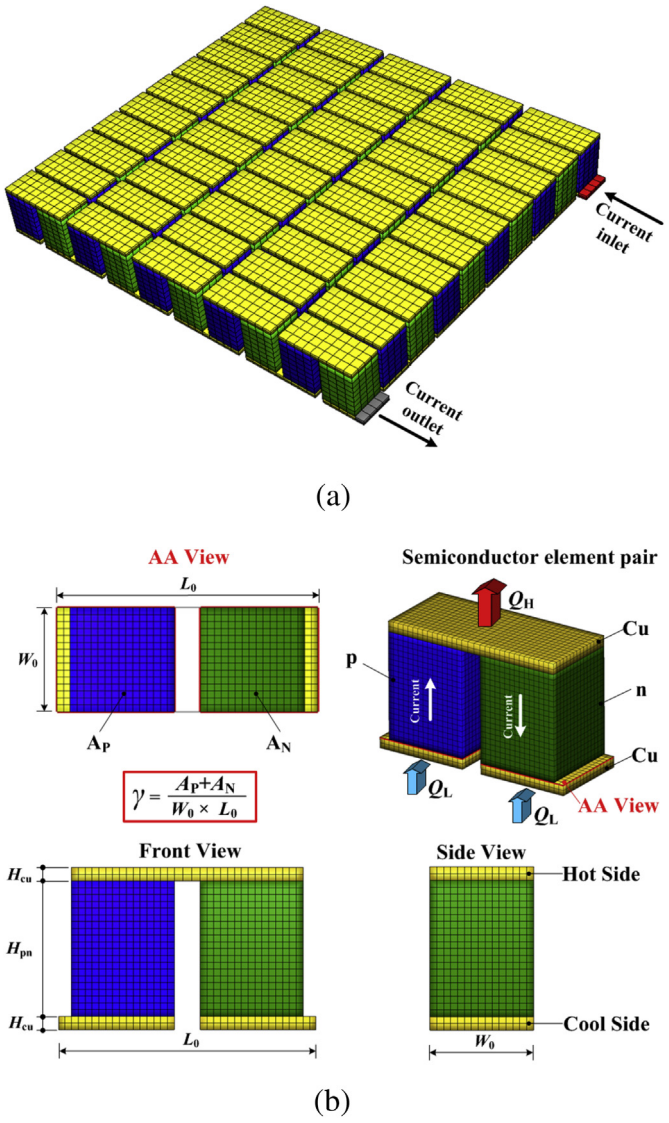

Fig. 1. Schematics of TEC and single semiconductor element pair: (a) TEC; (b) single semiconductor element pair.

different cross-sectional areas of p-type and n-type semiconductor columns. However, the present work does not account for this difference, and hence the same cross-sectional area of $A_p = A_n = A_{pn}$ is assumed as shown in Fig. 1b. The base area ratio of semiconductor columns to TEC is defined as $\gamma = N(A_p + A_n)/A_{total} = (A_p + A_n)/A_{pair}$, where A_{pair} is the pair area and equals $W_0 L_0$ (W_0 and L_0 are the width and length of a single pair, respectively). The copper interconnector has a thickness of H_{cu}. Once the semiconductor pair number N, the base area ratio γ, and the leg length H_{pn} are given, the TEC geometric structure is determined. Thus, these three parameters are chosen as the search variables and are optimized simultaneously to reach the maximum TEC cooling rate.

2.2. Direct problem model

The three-dimensional TEC model proposed by our pervious study [24] is adopted as direct problem model. The model assumes that the TEC is operated at steady-state; the p-type and n-type semiconductor columns are two separate parts and their material properties are temperature-dependent; the contact thermal resistance between semiconductor columns and metallic

interconnectors is ignored; and the heat loss by radiative and convective heat transfer to the ambient is ignored. The model includes the heat conduction equations and the electric potential equations, which are described briefly here and more details can be found in Ref. [24].

2.2.1. Heat conduction equations

$$\nabla\cdot(\lambda_i\nabla T)+\frac{j^2}{\sigma_i}-\beta_i\vec{j}\cdot\nabla T=0 \tag{1}$$

$$\nabla\cdot(\lambda_{\mathrm{p}}\nabla T)+\frac{j^2}{\sigma_{\mathrm{p}}}-\beta_{\mathrm{p}}\vec{j}\cdot\nabla T=0 \tag{2}$$

$$\nabla\cdot(\lambda_{\mathrm{n}}\nabla T)+\frac{j^2}{\sigma_{\mathrm{n}}}-\beta_{\mathrm{n}}\vec{j}\cdot\nabla T=0 \tag{3}$$

2.2.2. Electric potential equation

$$\nabla\cdot(\sigma(\nabla\phi-\alpha\nabla T))=0 \tag{4}$$

In the above equations, λ is the thermal conductivity, σ is the electric conductivity, β is the Thomson coefficient, $\vec{j}$ is the current density vector, α is the Seebeck coefficient, and ϕ is the electric potential. The subscripts i, p, and n denote the interconnector, p-type and n-type semiconductors, respectively. The Thomson coefficient can be related to the Seebeck coefficient as follows:

$$\beta=T\frac{\mathrm{d}\alpha}{\mathrm{d}T} \tag{5}$$

Once the electric potential is obtained, the current density vector can be calculated by the following equation, or:

$$\vec{j}=\sigma\vec{E}=\sigma(-\nabla\phi+\alpha\nabla T) \tag{6}$$

2.2.3. Boundary conditions

The constant temperatures T_H and T_L are applied at the hot and cold ends of the TEC. The temperature and heat flux are assumed to be continuous on the interface between the interconnector and semiconductor. The adiabatic boundary condition is assumed on the side surfaces of the TEC. The fixed applied current and zero electric potential are specified on the inlet and outlet of the TEC, and on the other surfaces the current cannot flow out the TEC.

2.2.4. Material properties

The thermoelectric materials $Bi_2(Te_{0.94}Se_{0.06})_3$ and $(Bi_{0.25}Sb_{0.75})Te_3$ are chosen as the n-type and p-type semiconductors, respectively. Their thermal conductivities, electric conductivities and Seebeck coefficients are all assumed to be temperature-dependent, or:

$$\lambda(T)=\lambda_0(T_0)\left[1+A_1(T-T_0)+A_2(T-T_0)^2\right] \tag{7}$$

$$\frac{1}{\sigma(T)}=\rho(T)=\rho_0(T_0)\left[1+B_1(T-T_0)+B_2(T-T_0)^2\right] \tag{8}$$

$$\alpha(T)=\alpha_0(T_0)\left[1+D_1(T-T_0)+D_2(T-T_0)^2\right] \tag{9}$$

where, the parameters are fitted based on the experimental data of Yamashita et al. [32] and are listed in Table 1. The copper is selected as the interconnector with constant properties due to its weak thermoelectric effect.

2.3. Inverse problem model

There are two parameters used to evaluate the TEC performance, the cooling rate Q_L and the COP (coefficient of performance). The cooling rate is defined as a heat adsorbed from the cold end, and the COP is defined as follows:

$$\mathrm{COP}=\frac{Q_L}{P}=\frac{Q_L}{IV} \tag{10}$$

where P is the electric power, I is the applied current, and V is the electric potential difference through the TEC.

For a TEC with a specific geometry, Q_L and COP are all dependent on its operating conditions: the temperature difference ($\Delta T=T_H-T_L$) and applied current. With a fixed ΔT, Q_L and COP are first increased and then decreased as I is increased. Unfortunately, the optimal applied currents corresponding to $Q_{L,\max}$ and $\mathrm{COP}_{\max}$ are not the same, which means that $Q_{L,\max}$ and $\mathrm{COP}_{\max}$ always cannot reach simultaneously [24]. Similarly, with the same operating conditions, as the TEC geometry is varied, Q_L and COP are all varied, but maybe cannot reach the maximums simultaneously. For practical cooling applications, the cooling rate is a priority. Hence, Q_L is chosen as the objective function in the present optimization, thus, an optimal set of geometric parameters is searched to reach the maximum Q_L. Because optimization of TEC geometry maybe causes the reduction in the COP, the COP is used as a constraint condition during the optimization in order to guarantee that the TEC with the optimal geometry has a relatively high COP. A value of COP that is not lower than 70% COP of the initial TEC geometry is chosen as the constraint condition here, or for all search steps:

$$\mathrm{COP}\geq 0.7\mathrm{COP}_{\mathrm{ini}} \tag{11}$$

It is worth noting that the selection of the value of 70% $\mathrm{COP}_{\mathrm{ini}}$ seems to be somewhat arbitrary, however, there is no universal standard to select a proper COP when Q_L is used as the objective function because Q_L and COP are two incomparable parameters to evaluate the TEC performance.

The simplified conjugate-gradient method is used as the inverse problem model in the present optimization approach. The simplified conjugate-gradient method evaluates the gradients of

Table 1
Parameters in Eqs. (7)–(9) for thermoelectric materials ($T_0=300$ K).

Material	Thermal conductivity			Electric resistivity			Seebeck coefficient		
	λ_0 (W m^{-1} K^{-1})	A_1 (K^{-1})	A_2 (K^{-2})	ρ_0 (Ω m)	B_1 (K^{-1})	B_2 (K^{-2})	α_0 (V K^{-1})	D_1 (K^{-1})	D_2 (K^{-2})
p-type	1.472	-1.29×10^{-3}	1.35×10^{-5}	8.826×10^{-6}	5.88×10^{-3}	8.93×10^{-6}	2.207×10^{-4}	1.55×10^{-3}	-3.15×10^{-6}
n-type	1.643	-9.80×10^{-4}	1.56×10^{-5}	8.239×10^{-6}	4.70×10^{-3}	2.67×10^{-6}	-2.23×10^{-4}	5.62×10^{-4}	-4.65×10^{-6}
Interconnector	400	0	0	1.7×10^{-9}	0	0	6.5×10^{-6}	0	0

the objective function and sets up a new conjugate direction for the updated search variables with the help of a sensitivity analysis. The details of the model can be found in our previous works [25–31]. The optimization procedure is described briefly in the following. For convenience, C_1, C_2 and C_3 are used to denote the semiconductor pair number N, the base area ratio γ, and the leg length H_{pn}, which are referred to as the search variables.

(1) Specify the initial guess for the search variables C_1–C_3 and the values of the search step sizes β_1–β_3.
(2) Create the geometry and grids of the TEC using the specified search variables C_1–C_3. Set up all boundary conditions, and then numerically solve Eqs. (1)–(6).
(3) Evaluate the objective function $J = Q_L$. When the convergence criterion is satisfied, the objective function reaches a maximum, then terminate iteration; otherwise, proceed to step (4).
(4) Evaluate the sensitivity coefficients $\partial J/\partial C_k$ (k = 1, 2, 3) of the objective function for each search variable based on the following equation:

$$\frac{\partial J}{\partial C_k} = \frac{\Delta J}{\Delta C_k} \tag{12}$$

It is noted that in step (4), the direct problem model is invoked three times to calculate $\partial J/\partial C_k$ ($k = 1, 2, 3$), respectively, by introducing a small perturbation ΔC_k into the search variable C_k ($k = 1, 2, 3$).

(5) Evaluate the conjugate-gradient coefficients γ_k (k = 1, 2, 3) for each search variable,

$$\gamma_k^{(n)} = \left[\frac{(\partial J/\partial C_k)^{(n)}}{(\partial J/\partial C_k)^{(n-1)}}\right]^2 \tag{13}$$

where, the superscripts n and $n-1$ denote the nth and $(n-1)$th search step, and for $n = 1$, $\gamma_k = 0$.

(6) Evaluate the search directions π_k (k = 1, 2, 3),

$$\pi_k^{(n)} = \left(\frac{\partial J}{\partial C_k}\right)^{(n)} + \gamma_k^{(n)}\pi_k^{(n-1)} \tag{14}$$

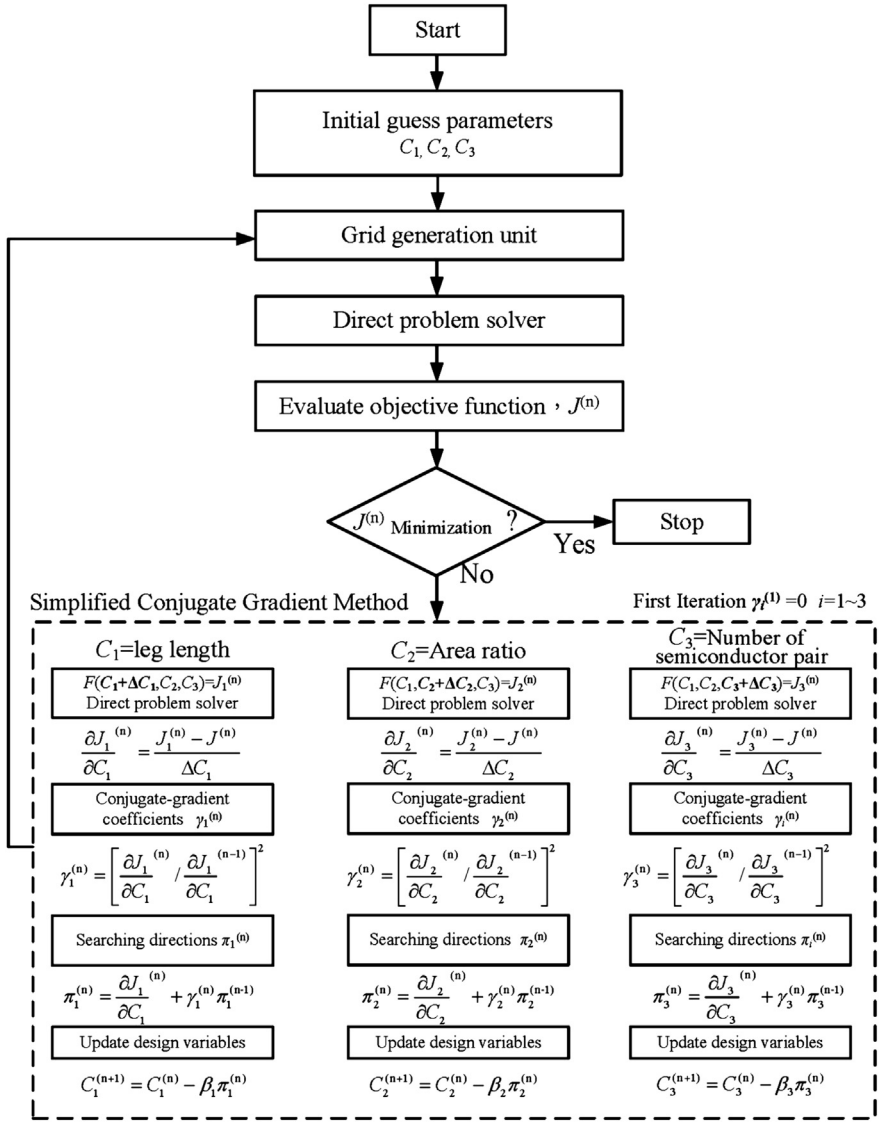

Fig. 2. Flow chart of optimization procedure.

(7) Update new search variables,

$$C_k^{(n+1)} = C_k^{(n)} - \beta_k \cdot \pi_k^{(n)} \quad (15)$$

and then return to step (2).

The typical values of ΔC_k ($k = 1, 2, 3$) are 1 for N, 0.002 for γ, and 0.05 mm for H_{pn}. The values of β_k ($k = 1, 2, 3$) varies from 0.001 to 0.01 depending on the convergence level during optimization. A flow chart of the optimization is shown in Fig. 2. In steps (2) and (4), the TEC model, Eqs. (1)–(6), are converted to the finite-difference form by the control volume method and are solved iteratively with an iteration criterion for convergence of 10^{-6}. The TEC model and simplified conjugate-gradient model are coupled and solved using a self-built Fortran program.

The TEC model has been validated in our previous works for the steady-state operation [24] and the transient operation [33], more details can be found in Refs. [24,33].

3. Results and discussion

3.1. The performance of TEC with initial geometry

A miniature TEC with the base area of only 3 × 3 mm^2 is selected as the testing example to display applicability of the present inverse problem approach to optimization of multi-parameters of TEC geometry. The initial design of the TEC has $N = 25$, $\gamma = 0.8$, and $H_{pn} = 0.5$ mm. The cold end temperature T_L is fixed to 300 K. The I–Q_L, I–COP, and I–P curves for various temperature differences are shown in Fig. 3. Fig. 3 confirms the statement in Section 2.2, with a fixed temperature difference $\Delta T > 0$, Q_L and COP are first increased and then decreased as I is increased, and there are two optimal applied currents at which the maximum Q_L and the maximum COP occur, respectively. To obtain a higher COP, a small current is recommended, however, Q_L is lower (Fig. 3a). Oppositely, a larger Q_L occurs at a relatively high current, however, at which COP is lower (Fig. 3b). Fig. 3 also shows that Q_L and COP at a large ΔT are lower than those at a small ΔT, hence, the hot end of the TEC generally is cooled by a heat sink to reach a better performance. The reduced COP at a large ΔT can be attributed to the increased electric power P (Fig. 3c) as well as the reduced cooling rate Q_L.

3.2. Individual parametric study for search variables

Before the optimization, an individual parameter analysis is performed to reveal the effects of H_{pn}, γ, and N on the TEC performance, as shown in Fig. 4. In the calculations, the temperatures of the cold and hot ends are all assumed to be 300 K with 0 K temperature difference. The applied current is taken as 1 A. The parameters for the base-line case (corresponding to the initial TEC geometry) are $H_{pn} = 0.5$ mm, $\gamma = 0.8$, and $N = 25$. In the individual parameter study, when a parameter is varied to evaluate its effect, other two parameters remain the same as with the base-line case. Fig. 4 shows that a small H_{pn} and a large γ will elevate Q_L of the TEC, however, an optimal $N = 49$ is observed at which the maximum Q_L is 3.52 W. The above results can be explained using the following relationship derived by zero-dimensional model [34],

$$Q_L = N\left[(\alpha_p - \alpha_n) I T_L - \frac{1}{2} I^2 \left(\frac{H_{pn}}{\sigma_p A_{pn}} + \frac{H_{pn}}{\sigma_n A_{pn}}\right) - \left(\frac{\lambda_p A_{pn}}{H_{pn}} + \frac{\lambda_n A_{pn}}{H_{pn}}\right)\Delta T\right] \quad (16)$$

where, the first, second, and third terms of the right side in Eq. (16) denote the heat absorbed from the cold end due to Peltier effect,

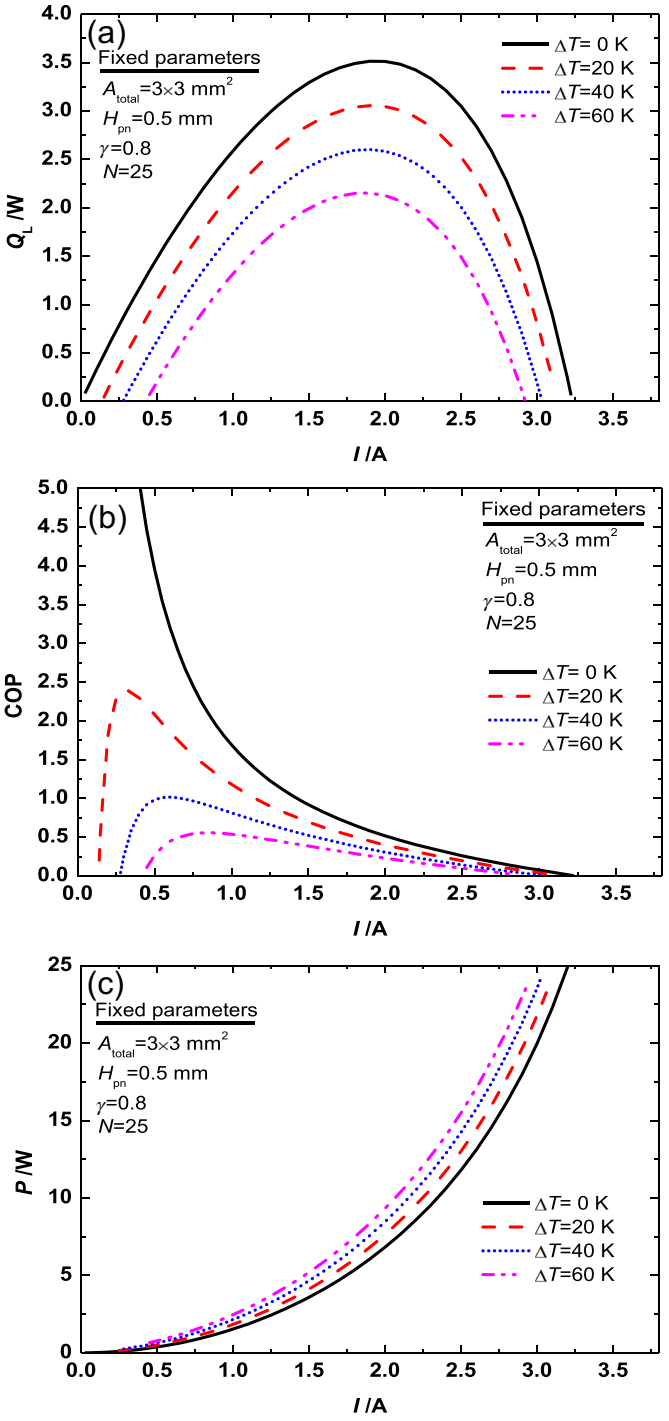

Fig. 3. Performance of TEC with initial geometry: (a) cooling rate; (b) COP; (c) electric power.

the heat transferred to the cold end due to Joule heating, and the heat transferred to the cold end due to Fourier's backward heat conduction. According to Eq. (16), when the temperature difference is $\Delta T = 0$ K, the third term equals zero, hence, the cooling rate Q_L is determined by subtracting the second term from the first term, thus, the increase in the first term and/or the decrease in the second term will elevate Q_L. With the same N and the same operating conditions ($I = 1$ A, $T_L = 300$ K, and $\Delta T = 0$ K), a small H_{pn} and a larger γ (corresponding to a large cross-sectional area of semiconductor column A_{pn}) mean a low electric resistance of the TEC

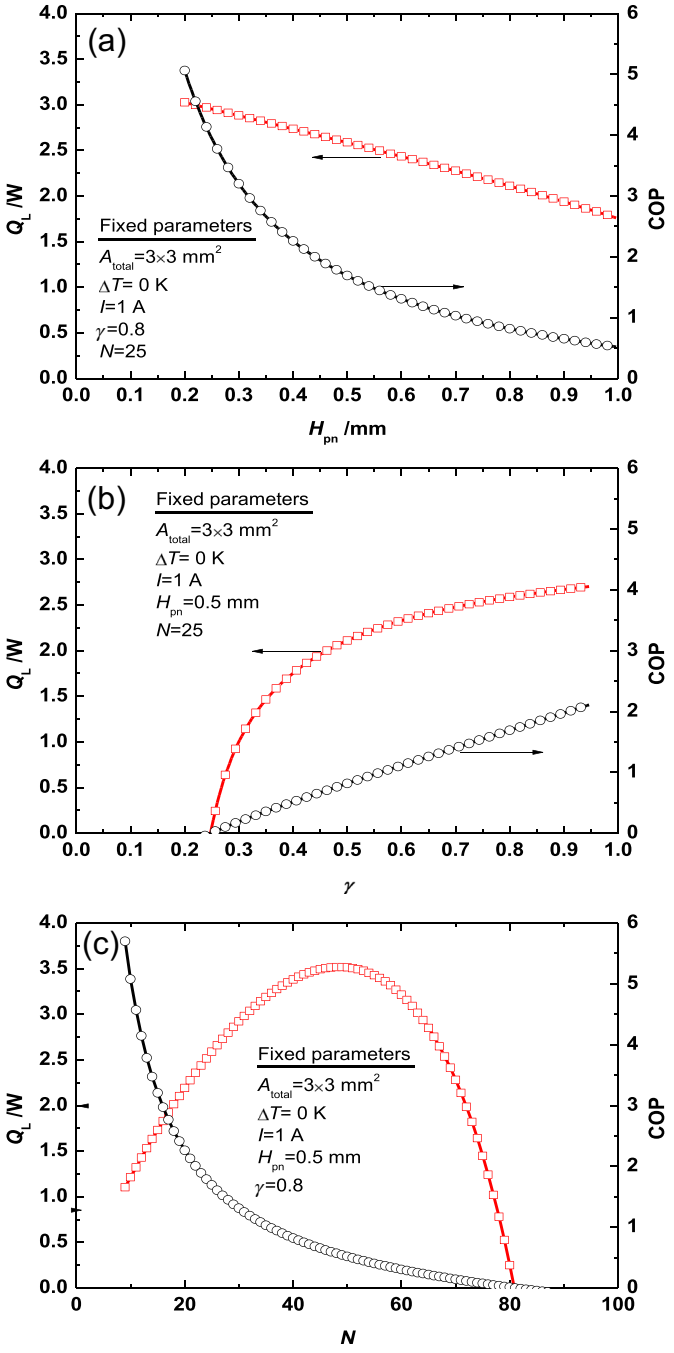

Fig. 4. The effect of individual parameter on TEC performance: (a) leg length H_{pn}; (b) base area ratio γ; (c) semiconductor pair number N.

and hence a low electric potential difference through the TEC (Fig. 5), thus, the Joule heating is weak which leads to a large Q_L. However, with the same H_{pn} and γ, a large N corresponds to a small A_{pn}, hence, the Peltier heat $N(\alpha_p-\alpha_n)IT_L$ and the heat transferred to the cold end 0.5 NH_{pn} $I^2(1/(\sigma_pA_{pn})+1/(\sigma_nA_{pn}))$ are all increased as N is increased. Therefore, increase in N has both positive and negative effect on the cooling rate, in other word, the cooling rate is non-monotonic function of N, thus, the optimal N corresponding to the maximum Q_L is dependent on competition of the first term and the second term. Different from Q_L, COP is always varied monotonously, a higher COP is observed at smaller H_{pn} and N, as well as at larger γ.

3.3. Three-parameter optimization of TEC geometry

The individual parameter study indicates that a small H_{pn} and a large γ improve Q_L of the TEC, however, H_{pn} cannot be arbitrarily small due to the constraint by practical processing technology, and γ cannot be equal to 1, hence, a constraint condition with $H_{pn} \geq 0.2$ mm and $\gamma \leq 0.95$ is adopted in the present optimization. It can be expected that the optimal geometry of the TEC should be varied at different operating conditions due to the dependence of Q_L and COP on the applied current and temperature difference. Therefore, the geometric parameters (N, γ, H_{pn}) of the TEC are

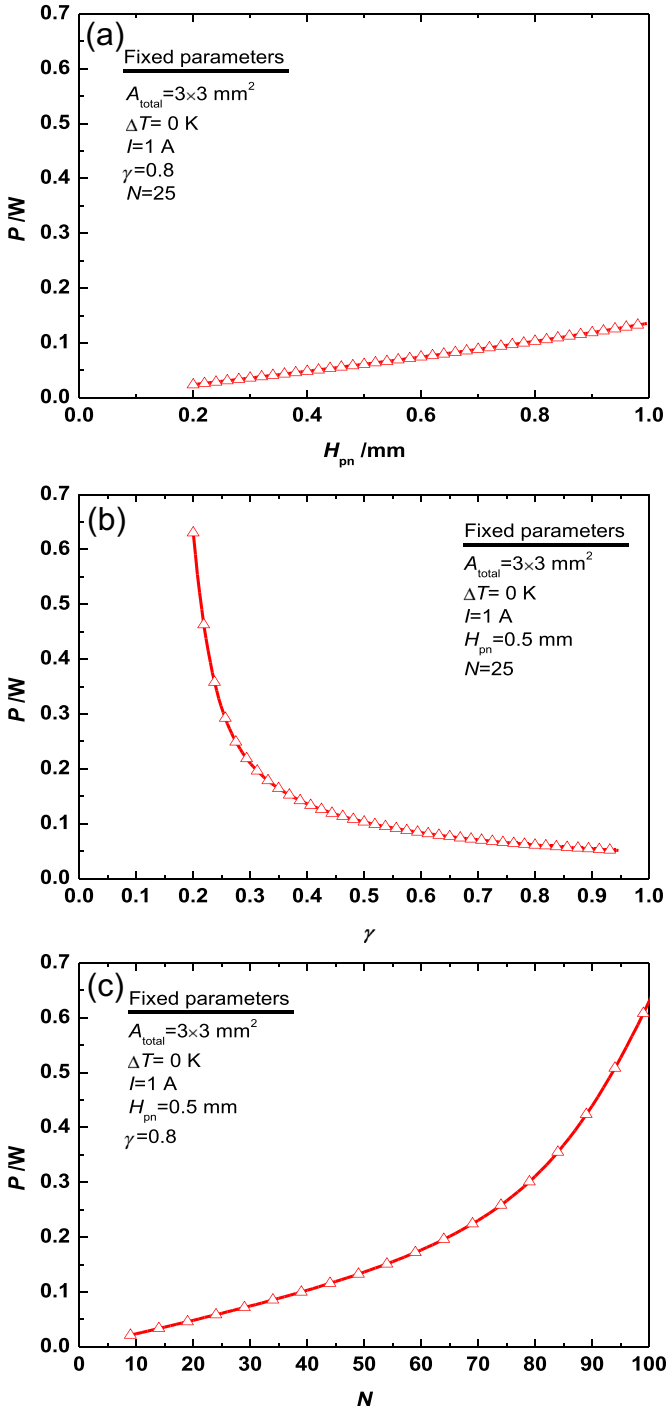

Fig. 5. Electric potential difference through the TEC for various geometric parameters: (a) leg length H_{pn}; (b) base area ratio γ; (c) semiconductor pair number N.

optimized to look for the maximum Q_L at operating conditions of $I = 0.5$ A, 1.0 A, 1.5 A, 2.0 A, 2.5 A, and 3.0 A as well as $\Delta T = 0$ K, 20 K, 40 K, and 60 K, respectively. It is worth noting that although $\Delta T = 0$ K is no practical meanings for refrigeration purpose, however, it can obtain the maximum Q_L for cooling purpose at the same TEC geometry and the same applied current.

3.3.1. Optimal design at $\Delta T = 0$ K

Fig. 6 shows the changes in three search variables for various I at $\Delta T = 0$ K during optimization. It can be seen that the search variables vary from their initial values of $H_{pn} = 0.5$ mm, $\gamma = 0.8$, and $N = 25$ as the search step number increases, and finally reach the optimal values. Optimal design has the same $\gamma = 0.95$ and $H_{pn} = 0.2$ mm, however, has different N at various applied currents I. It is noted that γ and H_{pn} for optimal design are equal to their constraint value, hence, when the base area of the TEC is fixed, to obtain the optimal cooling rate the leg length should be as small as possible and the total area of semiconductor columns should be as large as possible for a practical TEC design. Fig. 6c shows that the optimal N is 100 at $I = 0.5$ A, and it reduces to 95, 90, 72, 58, and 48 at $I = 1.0$ A, 1.5 A, 2.0 A, 2.5 A, and 3.0 A, respectively. This result can be explained as follows. Since the optimal design has the same $\gamma = 0.95$ and $H_{pn} = 0.2$ mm, a larger N means that the semiconductor column has a smaller cross-sectional area A_{pn}, which causes a higher electric resistance of the TEC and hence a stronger Joule heating. This effect becomes more significantly at higher I, the Joule heating reduces Q_L based on Eq. (16), thus, the optimal design at higher I approaches to reduce N to obtain the maximum Q_L, as compared to at lower I.

The variations of Q_L and COP for various I during optimization are shown in Fig. 7. Q_L increases with the search steps, it approaches a plateau of 5.56 W after 15 search steps for $I = 0.5$ A, about 276% higher than that for the initial design. For currents $I = 1.0$ A, 1.5 A, 2.0 A, 2.5 A, and 3.0 A, the optimal design has $Q_L = 9.12$ W, 10.36 W, 10.47 W, 10.46 W, and 10.46 W, about 252%, 214%, 198%, 243%, and 624% higher than that for the initial design, respectively.

The present optimization restricts COP at each search step to be not lower than 70% COP of the initial design (Eq. (11)). Fig. 7b shows that COP of the optimal design at small currents of $I \leq 1.5$ A

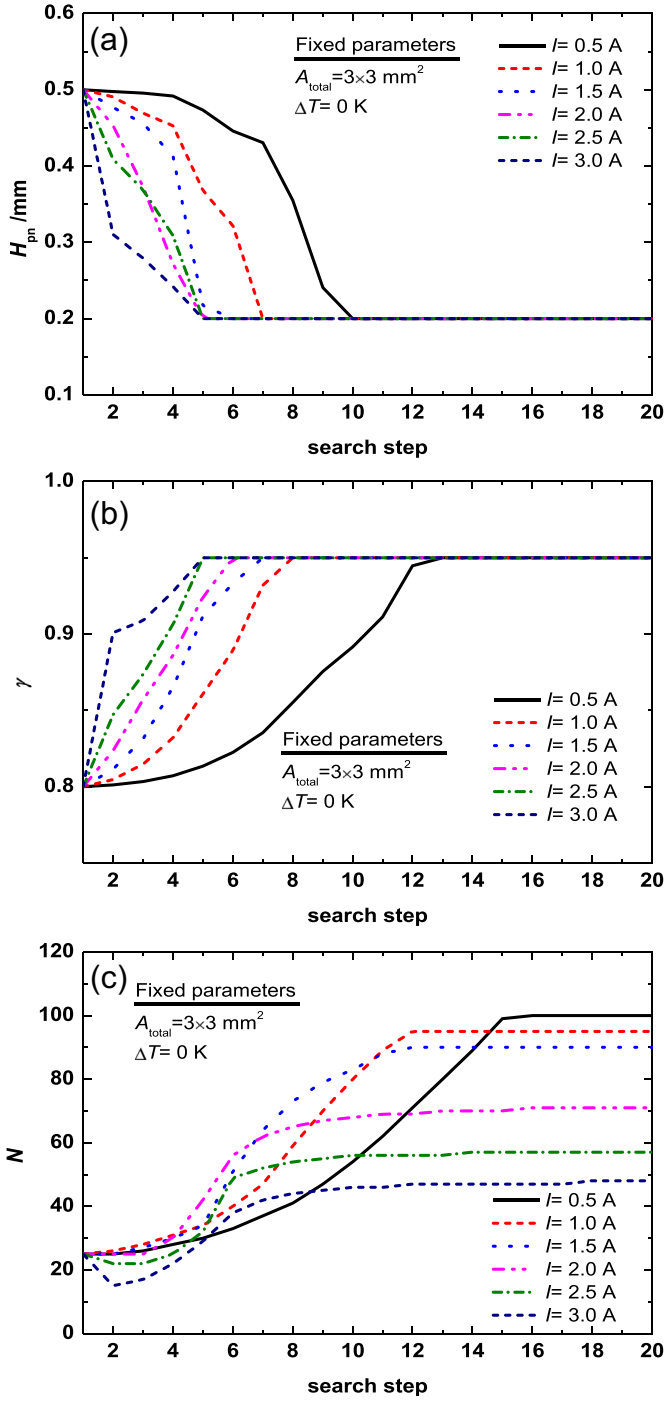

Fig. 6. Variations of search variables during optimization: (a) leg length H_{pn}; (b) base area ratio γ; (c) semiconductor pair number N.

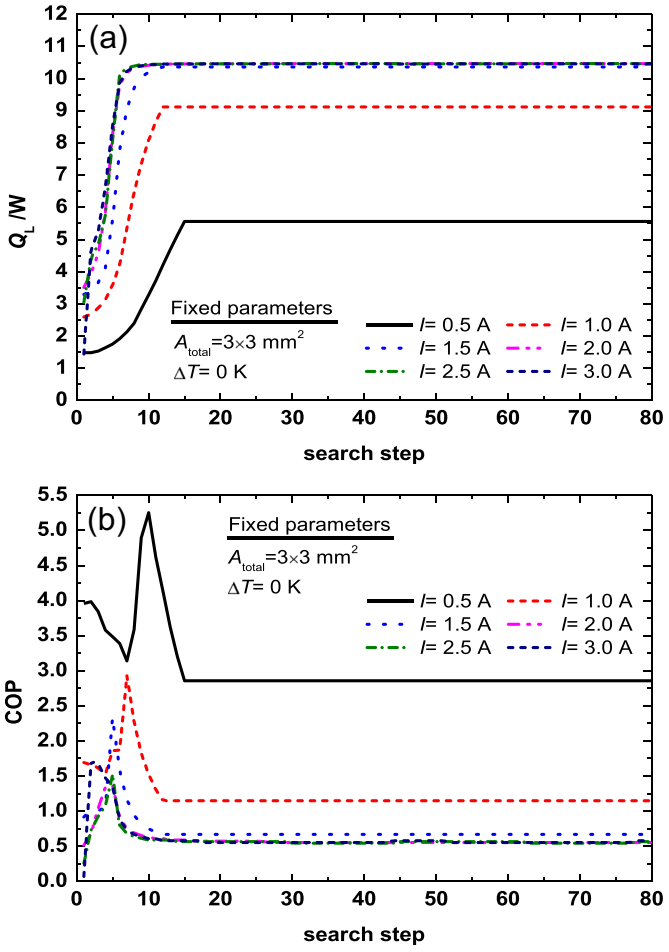

Fig. 7. Variations of TEC performance during optimization: (a) Q_L; (b) COP.

Table 2
The optimal semiconductor pair numbers for different temperature differences and applied currents.

I (A)	0.5	1.0	1.5	2.0	2.5	3.0
$\Delta T = 0$ K	100	95	90	72	58	48
$\Delta T = 20$ K	–	100	88	71	57	47
$\Delta T = 40$ K	–	110	89	70	56	46
$\Delta T = 60$ K	–	110	90	69	56	–

approaches this limit value. However, at large currents of $I \geq 2.0$ A, the optimal design has not only higher Q_L, but also higher COP than the initial design. It is noted that there is a peak value of COP during optimization as shown in Fig. 7b, which means that even for small applied currents, COP and Q_L can also be simultaneously higher than those of the initial design. For example, at $I = 0.5$ A, the initial design has COP = 3.96 and $Q_L = 1.48$ W, the design at tenth search step has COP = 5.25 and $Q_L = 3.28$ W, and the design at twelfth search step has COP = 4.13 and $Q_L = 4.21$ W. These two designs have lower Q_L but higher COP than the optimal design, hence, if large COP and Q_L are needed to be considered simultaneously for a specific application, these design can be selected.

3.3.2. *Effect of temperature difference on the optimal design*

Apart from the applied current I, the optimal TEC design is also dependent on the temperature difference ΔT. The three-parameter optimizations are also carried out at $\Delta T = 20$ K, 40 K, and 60 K with a fixed cold end temperature of $T_L = 300$ K. Similarly, the optimal design has $H_{pn} = 0.2$ mm and $\gamma = 0.95$. However, the optimal semiconductor pair number N is different for various ΔT and I, as shown in Table 2. At the same ΔT, a large N occurs at low applied current, and it decreases with the current increased, this phenomena has been explained in Section 3.3.1. At $I \leq 1.0$ A, a large N occurs at high temperature difference, however, at $I \geq 1.5$ A, N is almost independent on the temperature difference. This result is particularly useful for practical applications, since a sole optimal design can obtain the maximum cooling rate at various temperature differences.

Figs. 8 and 9 compare COP and Q_L of the optimal and initial designs at $\Delta T = 0$ K, 20 K, 40 K, and 60 K. Again, COP of the optimal design is lower at small currents $I \leq 1.5$ A, but is higher at large currents $I > 2.0$ A, as compared to that of the initial design (Fig. 8); However, Q_L is significantly increased for all temperature differences and applied currents (Fig. 9). It is noted that at the same ΔT, when $I > 2.0$ A almost the same COP and Q_L are obtained for the

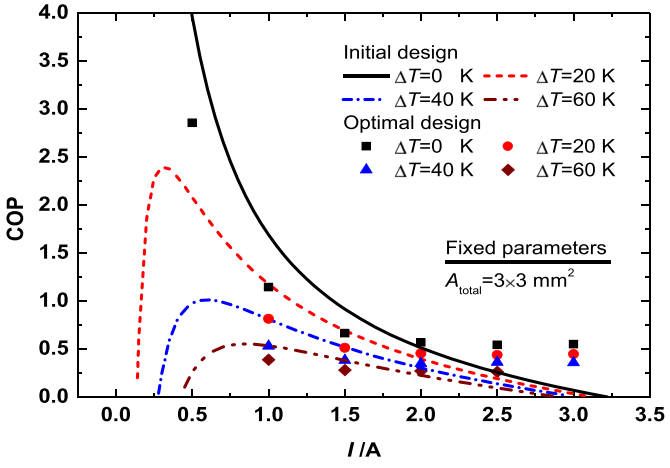

Fig. 8. Comparison of COP between the initial and optimal designs.

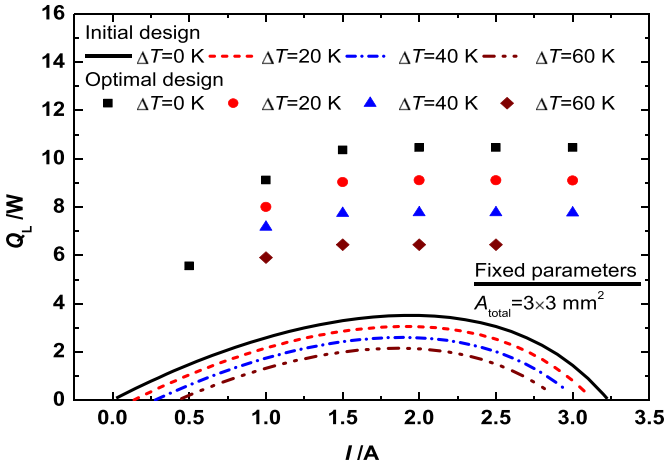

Fig. 9. Comparison of Q_L between the initial and optimal designs.

optimal design. Though the present optimization is carried out for a TEC with a specific base area of 3×3 mm^2, but the results obtained here provide a design direction, which is useful to guide the practical TEC design.

4. Conclusions

This work develops an optimization approach, which combines a simplified conjugate-gradient method and a complete three-dimensional TEC model, to look for optimal geometric structure of TECs. A miniature TEC with a base area of 3×3 mm^2 is used to test the optimization approach. The semiconductor pair number N, the leg length H_{pn}, and the base area ratio γ are adopted as search variables to maximum the objective function, defined as the cooling rate of the TEC. A value of COP that is not lower than 70% COP of the initial design at each search step is used as a constraint condition during optimization. The initial design has $N = 25$, $H_{pn} = 0.5$ mm, and $\gamma = 0.8$. The optimizations are carried out in a wide range of operating conditions: at temperature difference $\Delta T = 0$ K, 20 K, 40 K, and 60 K, as well as at applied current $I = 0.5$ A, 1.0 A, 1.5 A, 2.0 A, 2.5 A, and 3.0 A.

The optimal design has the same $H_{pn} = 0.2$ mm, and $\gamma = 0.95$ for all ΔT and I, which reach their limit values constrained by the present work, hence, when the base area of the TEC is fixed, to obtain the maximum cooling rate the leg length should be as small as possible and the total area of semiconductor columns should be as large as possible. The present optimizations also show that a large N is better to increase the cooling rate of the TEC at small currents and high temperature differences. At small currents of $I \leq 1.5$ A, improved cooling rate for the optimal design is at the expense of reduced COP, however, at large currents of $I > 2.0$ A, both the cooling rate and the COP can be increased significantly by searching for the optimal design.

Although the combined optimization is proven effective only for the miniature TEC with the base area of 3×3 mm^2, it is expected that the proposed design strategy is likely applicable to designs of the practical TEC with larger base area.

Acknowledgment

This study was supported by the National Natural Science Foundation of China (No. 51276060), by the 111 Project (No. B12034), by Program for New Century Excellent Talents in University (No. NCET-11-0635), and by the Fundamental Research Funds for the Central Universities (No. 11ZG01).

References

[1] Rezania A, Rosendahl LA. Thermal effect of a thermoelectric generator on parallel microchannel heat sink. Energy 2012;37:220–7.
[2] Chen WH, Liao CY, Hung CI, Huang WL. Experimental study on thermoelectric modules for power generation at various operating conditions. Energy 2012;45:874–81.
[3] Astrain D, Vian JG, Martinez A, Rodriguez A. Study of the influence of heat exchangers' thermal resistances on a thermoelectric generation system. Energy 2010;35:602–10.
[4] Martinez A, Astrain D, Rodríguez A. Experimental and analytical study on thermoelectric self cooling of devices. Energy 2011;36:5250–60.
[5] Martínez A, Astrain D, Rodríguez A. Dynamic model for simulation of thermoelectric self cooling applications. Energy 2013;55:1114–26.
[6] Riffat SB, Ma X. Thermoelectrics: a review of present and potential applications. Applied Thermal Engineering 2003;23:913–35.
[7] Minnich AJ, Dresselhaus MS, Ren ZF, Chen G. Bulk nanostructured thermoelectric materials: current research and future prospects. Energy & Environmental Science 2009;2:466–79.
[8] Völklein F, Min G, Rove DM. Modeling of microelectromechanical thermoelectric cooler. Sensors and Actuators 1999;75:95–101.
[9] Huang BJ, Chin CJ, Duang CL. A design method of thermoelectric cooler. International Journal of Refrigeration 2000;23:208–18.
[10] Xuan XC, Ng KC, Yap C, Chua HT. A general model for studying effects of interface layers on thermoelectric devices performance. International Journal of Heat and Mass Transfer 2002;45:5159–70.
[11] Huang MJ, Yen RH, Wang AB. The influence of the Thomson effect on the performance of a thermoelectric cooler. International Journal of Heat and Mass Transfer 2005;48:413–8.
[12] Cheng YH, Shih C. Maximizing the cooling capacity and COP of two-stage thermoelectric coolers through genetic algorithm. Applied Thermal Engineering 2006;26:937–47.
[13] Pan Y, Lin B, Chen J. Performance analysis and parametric optimal design of an irreversible multi-couple thermoelectric refrigerator under various operating conditions. Applied Energy 2007;84:882–92.
[14] Lee KH, Kim OJ. Analysis on the cooling performance of the thermoelectric microcooler. International Journal of Heat and Mass Transfer 2007;50:1982–92.
[15] Yu J, Wang B. Enhancing the maximum coefficient of performance of thermoelectric cooling modules using internally cascaded thermoelectric couples. International Journal of Refrigeration 2009;32:32–9.
[16] Chen WH, Liao CY, Huang CI. A numerical study on the performance of miniature thermoelectric cooler affected by Thomson effect. Applied Energy 2012;89:464–73.
[17] Chen L, Li J, Sun F, Wu C. Performance optimization of a two-stage semiconductor thermoelectric-generator. Applied Energy 2005;82:300–12.
[18] Meng F, Chen L, Sun F. A numerical model and comparative investigation of a thermoelectric generator with multi-irreversibilities. Energy 2011;36:3513–22.
[19] Wang CC, Hung CI, Chen WH. Design of heat sink for improving the performance of thermoelectric generator using two-stage optimization. Energy 2012;39:236–45.
[20] Meng F, Chen L, Sun F. Multivariable optimization of a two-stage thermoelectric refrigerator driven by a two-stage thermoelectric generator with external heat transfer. Indian Journal of Pure & Applied Physics 2010;48:731–42.
[21] Chen J, Lin B, Wang H, Lin G. Optimal design of a multi-couple thermoelectric generator. Semiconductor Science and Technology 2000;15:184–8.
[22] Chen G. Theoretical efficiency of solar thermoelectric energy generators. Journal of Applied Physics 2011;109:104908.
[23] Cheng YH, Lin WK. Geometric optimization of thermoelectric coolers in a confined volume using genetic algorithms. Applied Thermal Engineering 2005;25:2983–97.
[24] Wang XD, Huang YX, Cheng CH, Lin TW, Kang CH. A three-dimensional numerical modeling of thermoelectric device with consideration of coupling of temperature field and electric potential field. Energy 2012;47:488–97.
[25] Cheng CH, Chang MH. A simplified conjugate-gradient method for shape identification based on thermal data. Numerical Heat Transfer 2003;43:489–507.
[26] Wang XD, Huang YX, Cheng CH, Jang JY, Lee DJ, Yan WM, et al. An inverse geometry design problem for optimization of single serpentine flow field of PEM fuel cell. International Journal of Hydrogen Energy 2010;35:4247–57.
[27] Wang XD, Huang YX, Cheng CH, Jang JY, Lee DJ, Yan WM, et al. Flow field optimization for proton exchange membrane fuel cells with varying channel heights and widths. Electrochimica Acta 2009;54:5522–30.
[28] Jang JY, Cheng CH, Huang YX. Optimal design of baffles locations with interdigitated flow channels of a centimeter-scale proton exchange membrane fuel cell. International Journal of Heat and Mass Transfer 2010;53:732–43.
[29] Wang ZH, Wang XD, Yan WM, Duan YY, Lee DJ, Xu JL. Multi-parameters optimization for microchannel heat sink using inverse problem method. International Journal of Heat and Mass Transfer 2011;54:2811–9.
[30] Wang XD, An B, Xu JL. Optimal geometric structure for nanofluid-cooled microchannel heat sink under various constraint conditions. Energy Conversion and Management 2013;65:528–38.
[31] Lin TW. Optimization of the shell-and-tube heat exchanger by simplified conjugated gradient method. Advanced Science Letters 2012;9:451–5.
[32] Yamashita O, Sugihara S. High-performance bismuth-telluride compounds with highly stable thermoelectric figure of merit. Journal of Materials Science 2005;40:6439–44.
[33] Meng JH, Wang XD, Zhang XX. Transient modeling and dynamic characteristics of thermoelectric cooler. Applied Energy 2013;108:340–8.
[34] Xuan XC. Analyses of the performance and polar characteristics of two-stage thermoelectric coolers. Semiconductor Science and Technology 2002;17:414–20.